Magnetic oscillation modes in square lattice artificial spin ice

Thomas D. Lasnier* and G. M. Wysin†
Department of Physics, Kansas State University, Manhattan, KS 66506-2601
(Dated: May 27, 2020)

Small amplitude dipolar oscillations are considered in artificial spin ice on a square lattice in two dimensions. The net magnetic moment of each elongated magnetic island in the spin ice is assumed to have Heisenberg-like dynamics and be influenced by shape anisotropies and nearest neighbor dipole interactions. The magnetic dynamics linearized around a ground state with four sublattices leads to an eigenvalue problem with four branches of magnetic spin wave modes. An energy analysis of the dipole motions enables an analytic solution while showing that the lowest frequency modes are antisymmetric with regard to their in-plane dynamic fluctuations in each four-island vertex. Although only the leading dipolar interactions are included, modes similar to these may be observable experimentally in artificial square spin ice.

PACS numbers: 75.75.+a, 85.70.Ay, 75.10.Hk, 75.40.Mg
Keywords: magnetics, spin-ice, frustration, dipole interactions, magnon modes, spin waves.

I. INTRODUCTION: SQUARE SPIN ICE AND ITS DYNAMICS

Nanostructured arrays of thin elongated magnetic islands on a substrate, known as artificial spin ices, have received a lot of theoretical and experimental interest because of their unique properties and possibilities for technological applications[1]. The magnetic islands are typically created out of Permalloy, although other materials have been used. These islands possess an Ising-like dipole moment that tends to point in one of two directions parallel to the long axis of the island. The arrays are manufactured in a desired geometry that has built-in frustration, where all pairwise dipolar interactions cannot be simultaneously minimized [2]. For square lattice artificial spin ice, the lowest energy configuration at a vertex between four neighboring dipoles follows an *ice rule*: two dipoles point inward and two dipoles point outward at a vertex [3]. This leads to a doubly degenerate ground state as depicted in Fig. 1 where each vertex follows the ice rule, although it may be very difficult to achieve simply by cooling the sample [4]. This is distinct from the six-fold degenerate ground state of tetrahedral spin ice due to the fact that the spins are not equidistant in the square lattice. Six-fold degeneracy can be restored by adding a height offset to the lattice.[5, 6] Reversal of dipoles in a ground state leads to the generation of topological excitations that resemble magnetic monopoles, and are connected by energetic string excitations [4, 7–9].

If only dipolar interactions are considered in Monte Carlo simulations for an Ising spin ice model [7, 8, 10], annealing of the system from high towards low temperature brings it to a ground state. That approach leaves out the energy barriers involved in dynamic reversal. Each island has a strong easy-axis anisotropy that maintains the dipole's direction close to the island's long axis, as well as a strong easy-plane anisotropy maintaining the dipole's direction near the plane of the substrate. The energy associated with shape anisotropy of the islands is rather large compared to both the dipolar interactions and thermal energy scales [11, 12]. This means that reversal of individual dipoles is difficult by thermal activation, because some dipole reversals can be easily blocked by the anisotropy barriers, making it difficult for the system to relax into a ground state [13, 14] unless fields are applied. However thermal relaxation to a ground state has been observed experimentally using special protocols[15, 16].

The dynamics that is associated with lowest frequency spin waves is especially relevant for understanding the stability and signatures of different magnetic configurations as well as transitions among configurations. Here we consider the linearized dynamics out of a ground state configuration (sometimes called a vortex state), where no monopole excitations are present. Due to strong exchange interactions among the atomic spins within each island, we assume the that the net island dipoles have nearly constant magnitude, while moving in an anisotropy potential due to shape anisotropy, as considered in Ref. [11]. Iacocca *et al.* [17] refer to this as a *macrospin* approximation, where they used a semi-analytic approach including diagonalization and micromagnetics for finding various modes of oscillation in artificial square spin ice. Other studies of oscillation modes[18, 19] have been carried out to demonstrate how the mode spectrum is affected by the presence or absence of topological excitations, such as monopoles. Arroo *et al.* [20] studied the connection between magnetic configuration and spin wave spectra using micromagnetics on a small number of islands.

The model used here for spin waves in artificial ice assumes that the island dipoles (1) maintain a constant magnitude μ while rotating uniformly and (2) interact only with nearest neighbors. The first approximation requires strong ferromagnetic exchange within the islands,

*Electronic address: tdlasnier@k-state.edu
†Electronic address: wysin@phys.ksu.edu; URL: http://www.phys.ksu.edu/personal/wysin

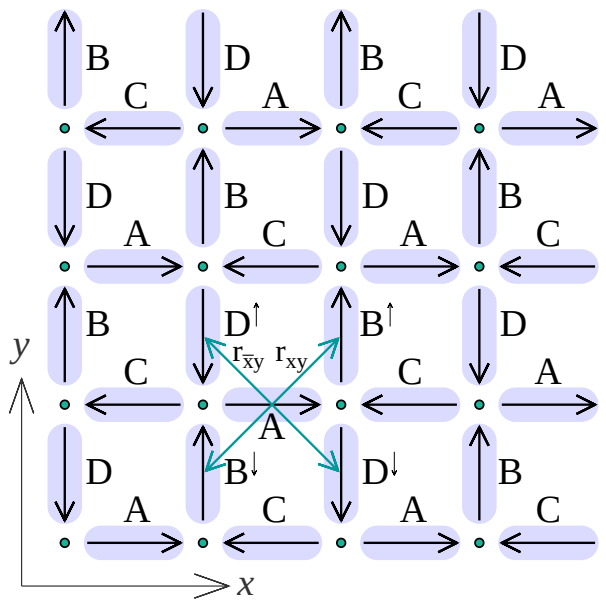

FIG. 1: Square spin ice in a ground state, with the identification of the four sublattices. Small dots indicate the vertices, at which the two-in/two-out rule holds. For one A-site its nearest neighbors are labeled $\mathbf{D}^{\uparrow}$, $\mathbf{D}^{\downarrow}$, $\mathbf{B}^{\uparrow}$ and $\mathbf{B}^{\downarrow}$ and the diagonal displacements $\mathbf{r}_{\rm xy}$ and $\mathbf{r}_{\bar{\rm x}\rm y}$ are indicated, see Eq. (6). The island lattice constant along diagonal directions is $a_{\rm I} = a/\sqrt{2}$, where a is the vertex lattice constant.

but tends to overestimate the island interactions and mode stiffness, while the second approximation tends to underestimate the island interactions. Both help to facilitate the analytic computation. The dipole moments are assumed to behave with continuous dynamics, as Heisenberg-like magnetic moments that can point in any direction, as considered in previous studies of thermally excited spin ice [12, 21]. The small-amplitude spin wave deviations away from a ground state will be important for use as a ground state signature, and to indicate what applied field frequencies and wave vectors will be able to reorganize a configuration.

The spin wave modes are determined as follows. In Sec. II the square lattice spin ice model is summarized. In Sec. III the dynamics for the nearest neighbor dipolar coupling is described. The system obtained is linearized in Sec. IV and the details of the modes found are given. Some excitation spectra for different model parameters are described in Sec. V, and results are summarized and their importance is highlighted in Sec. VI.

II. ARTIFICIAL SQUARE LATTICE SPIN-ICE MODEL

The islands' dipoles are assumed to have fixed magnitudes μ pointing along some time dependent Heisenberg-like unit vectors $\hat{\boldsymbol{\mu}}_i(t)$, where i labels a site. The directions of the $\hat{\boldsymbol{\mu}}_i(t)$ are affected by magnetic shape anisotropy and by long-range dipolar interactions. Due to the elongated form of the islands, each island has some uniaxial anisotropy with energy constant K_1 along its longer axis $\hat{\mathbf{u}}_i$, which points along either $\hat{\mathbf{x}}$ or $\hat{\mathbf{y}}$, depending on the sublattice. A sketch of the system is shown in Fig. 1. In addition, the islands are very thin perpendicular to the substrate, which makes that direction a hard axis, producing easy-plane (xy) anisotropy with an energy constant K_3 for all the islands. In Ref. [11], micromagnetics for an individual island indicates that the easy-plane anisotropy constant K_3 dominates, followed by the easy-axis interactions K_1, and then finally by the much weaker dipolar interactions.

The Hamiltonian for this model with Heisenberg-like island spins $\hat{\boldsymbol{\mu}}_i(t)$ is

$$\mathcal{H} = -\frac{\mu_0}{4\pi}\frac{\mu^2}{a^3}\sum_{i>j}\frac{[3(\hat{\boldsymbol{\mu}}_i\cdot\hat{\mathbf{r}}_{ij})(\hat{\boldsymbol{\mu}}_j\cdot\hat{\mathbf{r}}_{ij})-\hat{\boldsymbol{\mu}}_i\cdot\hat{\boldsymbol{\mu}}_j]}{(r_{ij}/a)^3} + \sum_i\left\{K_1[1-(\hat{\boldsymbol{\mu}}_i\cdot\hat{\mathbf{u}}_i)^2]+K_3(\hat{\boldsymbol{\mu}}_i\cdot\hat{\mathbf{z}})^2\right\} \quad (1)$$

The first term is the dipolar pair interaction, where μ_0 is the magnetic permeability of space, a is the center-to-center spacing of the islands along the $\hat{\mathbf{x}}$ or $\hat{\mathbf{y}}$ principal directions, and $\hat{\mathbf{r}}_{ij}$ is a unit vector pointing from site j to site i. Note, however, that the nearest neighbor spacing of the islands, $a_{\rm I} = a/\sqrt{2}$, lies along the $\pm\mathbf{r}_{xy}$ and $\pm\mathbf{r}_{\bar{x}y}$ directions at $\pm 45^\circ$ from the standard xy coordinate system, see Fig. 1. The dipolar energy scale is affected by island spacing, such that we define a nearest neighbor dipolar energy constant,

$$\mathcal{D} \equiv \frac{\mu_0}{4\pi}\frac{\mu^2}{a_{\rm I}^3}. \quad (2)$$

The anisotropy terms have been written so that they give zero energy when the island dipole points along its local easy-axis $\hat{\mathbf{u}}_i$. Rotation of $\hat{\boldsymbol{\mu}}_i(t)$ within the xy plane only involves the K_1 energy, whereas, tilting of $\hat{\boldsymbol{\mu}}_i(t)$ out of the xy-plane is characterized by the sum of the two anisotropy constants, $K_1 + K_3$.

A. The spin-ice ground states

In a ground state, such as in Fig. 1, the shape anisotropy energies are totally minimized but the nearest neighbor dipolar interactions are frustrated. The magnetic moments alternate in direction from site to site. We assume four sublattices, A,B,C,D. The A and C sites are aligned with $+\hat{\mathbf{x}}$ and $-\hat{\mathbf{x}}$, respectively, due to having in-plane anisotropy axes $\hat{\mathbf{u}}_i = \hat{\mathbf{x}}$. The B and D sites are aligned with $+\hat{\mathbf{y}}$ and $-\hat{\mathbf{y}}$, respectively, due to having in-plane anisotropy axes $\hat{\mathbf{u}}_i = \hat{\mathbf{y}}$. In a ground state, the unit island dipoles $\hat{\boldsymbol{\mu}}_i$ on the sublattices are

$$\mathbf{A}_0 = (\ 1, 0, 0), \quad \mathbf{B}_0 = (0, 1, 0), \quad (3a)$$
$$\mathbf{C}_0 = (-1, 0, 0), \quad \mathbf{D}_0 = (0, -1, 0). \quad (3b)$$

The other ground state would be obtained from this one by inverting all the moments. There is an enormous energy barrier preventing that transition. Instead, here we consider only small spatially periodic deviations away from this ground state configuration, characterized by some two-dimensional wave vector $\mathbf{q} = (q_x, q_y)$.

III. THE DYNAMICS AND SYMMETRIES

The dynamic equation of motion for the magnetic moment of some island, regardless of which sublattice it occupies, results from the Hamiltonian according to a torque equation,

$$\frac{d\hat{\boldsymbol{\mu}}_i}{dt} = \gamma_{\rm e}\hat{\boldsymbol{\mu}}_i \times \mathbf{B}_i. \tag{4}$$

where $\gamma_{\rm e}$ is a gyromagnetic ratio. Based on the local energies at each site, there is an effective magnetic field that acts on the island at a site,

$$\begin{aligned}\mathbf{B}_i &= -\frac{\partial \mathcal{H}}{\partial \boldsymbol{\mu}_i} = -\frac{1}{\mu}\frac{\partial \mathcal{H}}{\partial \hat{\boldsymbol{\mu}}_i} = \frac{\mathcal{D}}{\mu}\sum_{j\neq i}\frac{3(\hat{\boldsymbol{\mu}}_j\cdot\hat{\mathbf{r}}_{ij})\hat{\mathbf{r}}_{ij} - \hat{\boldsymbol{\mu}}_j}{(r_{ij}/a)^3} \\ &+ 2\frac{K_1}{\mu}(\hat{\boldsymbol{\mu}}_i\cdot\hat{\mathbf{u}}_i)\hat{\mathbf{u}}_i - 2\frac{K_3}{\mu}(\hat{\boldsymbol{\mu}}_i\cdot\hat{\mathbf{z}})\hat{\mathbf{z}}.\end{aligned} \tag{5}$$

In general, the anisotropy fields are local while the dipolar interactions extend through the entire lattice.

A. Nearest neighbor dipolar model

Although the dipolar interactions are long-ranged, in order to make initial progress and keep this calculation tractable, only nearest neighbor dipolar couplings are included. This approximation has previously been used for artificial spin ice with good results, however there are instances where it fails to fully capture the behavior of the system[22, 23]. The general properties of the solutions should not be significantly altered by this approximation, although the exact values will certainly be different. To develop the equations for the undamped dynamics, we consider first a site on the A-sublattice, and its interactions with the nearest neighbors on the B-sublattice and the D-sublattice, see Fig. 1. An arbitrary A-site couples to two B-sites whose unit dipoles are labeled as $\mathbf{B}^{\uparrow}$ and $\mathbf{B}^{\downarrow}$, and two D-sites whose unit dipoles are labeled as $\mathbf{D}^{\uparrow}$ and $\mathbf{D}^{\downarrow}$, where the arrows $(\uparrow,\downarrow)$ indicate the y-direction of the space displacement from the A-site. To be specific, the displacements from the A-site to these neighbors are

$$\mathbf{r}_{\rm AB^{\uparrow}} = \mathbf{r}_{\rm xy} \equiv (\ \tfrac{a}{2}, \tfrac{a}{2}, 0), \quad \mathbf{r}_{\rm AB^{\downarrow}} = -\mathbf{r}_{\rm xy}, \tag{6a}$$
$$\mathbf{r}_{\rm AD^{\uparrow}} = \mathbf{r}_{\bar{\rm x}\rm y} \equiv (-\tfrac{a}{2}, \tfrac{a}{2}, 0), \quad \mathbf{r}_{\rm AD^{\downarrow}} = -\mathbf{r}_{\bar{\rm x}\rm y}. \tag{6b}$$

These displacements have length $a_{\rm I} = a/\sqrt{2}$, the island lattice constant. From (4), the dynamic equation for the time derivative of the A-site unit dipole $\hat{\boldsymbol{\mu}}_i \equiv \mathbf{A}$ can be expressed as

$$\frac{d\mathbf{A}}{dt} = \mathbf{A}\times\mathbf{F}(\rm A), \tag{7}$$

where the effective field $\mathbf{F}(\rm A)$ acting on that site includes local anisotropy terms and only the nearest neighbor dipolar terms,

$$\begin{aligned}\mathbf{F}(\rm A) &= \kappa_1 A_x\hat{\mathbf{x}} - \kappa_3 A_z\hat{\mathbf{z}} \\ &+\delta_1\Big\{3\left[(\mathbf{B}^{\uparrow}+\mathbf{B}^{\downarrow})\cdot\hat{\mathbf{r}}_{\rm xy}\right]\hat{\mathbf{r}}_{\rm xy} - \mathbf{B}^{\uparrow} - \mathbf{B}^{\downarrow} \\ &\quad +3\left[(\mathbf{D}^{\uparrow}+\mathbf{D}^{\downarrow})\cdot\hat{\mathbf{r}}_{\bar{\rm x}\rm y}\right]\hat{\mathbf{r}}_{\bar{\rm x}\rm y} - \mathbf{D}^{\uparrow} - \mathbf{D}^{\downarrow}\Big\}.\end{aligned} \tag{8}$$

The constants κ_1, κ_3, and δ_1 have dimensions of frequency and are defined as

$$\kappa_1 \equiv \frac{2\gamma_{\rm e}K_1}{\mu}, \quad \kappa_3 \equiv \frac{2\gamma_{\rm e}K_3}{\mu}, \quad \delta_1 \equiv \frac{\gamma_{\rm e}\mathcal{D}}{\mu}. \tag{9}$$

Once the nearest neighbor displacements are substituted into (8), the components of $\mathbf{F}(\rm A)$ are found to be

$$\begin{aligned}F_x(\rm A) &= \delta_1\left[\tfrac{1}{2}\left(B_x^{\uparrow}+B_x^{\downarrow}+D_x^{\uparrow}+D_x^{\downarrow}\right)\right. \\ &\quad \left.+\tfrac{3}{2}\left(B_y^{\uparrow}+B_y^{\downarrow}-D_y^{\uparrow}-D_y^{\downarrow}\right)\right] + \kappa_1 A_x, \quad \text{(10a)} \\ F_y(\rm A) &= \delta_1\left[\tfrac{1}{2}\left(B_y^{\uparrow}+B_y^{\downarrow}+D_y^{\uparrow}+D_y^{\downarrow}\right)\right. \\ &\quad \left.+\tfrac{3}{2}\left(B_x^{\uparrow}+B_x^{\downarrow}-D_x^{\uparrow}-D_x^{\downarrow}\right)\right], \quad \text{(10b)} \\ F_z(\rm A) &= -\delta_1\left(B_z^{\uparrow}+B_z^{\downarrow}+D_z^{\uparrow}+D_z^{\downarrow}\right) - \kappa_3 A_z. \quad \text{(10c)}\end{aligned}$$

By the symmetry of the lattice, a C-site follows a dynamic equation of the same form as in (7) and (8), with its field $\mathbf{F}(\rm C)$ obtained using the replacements $\mathbf{A}\to\mathbf{C}$, $\mathbf{B}\to\mathbf{D}$ and $\mathbf{D}\to\mathbf{B}$, and relations just like (6) for the displacements:

$$\mathbf{r}_{\rm CD^{\uparrow}} = \mathbf{r}_{\rm xy} \equiv (\ \tfrac{a}{2}, \tfrac{a}{2}, 0), \quad \mathbf{r}_{\rm CD^{\downarrow}} = -\mathbf{r}_{\rm xy}, \tag{11a}$$
$$\mathbf{r}_{\rm CB^{\uparrow}} = \mathbf{r}_{\bar{\rm x}\rm y} \equiv (-\tfrac{a}{2}, \tfrac{a}{2}, 0), \quad \mathbf{r}_{\rm CB^{\downarrow}} = -\mathbf{r}_{\bar{\rm x}\rm y}. \tag{11b}$$

Similarly, with a B-site having a long axis along $\hat{\mathbf{y}}$, the effective field for its dynamics is

$$\begin{aligned}\mathbf{F}(\rm B) &= \kappa_1 B_y\hat{\mathbf{y}} - \kappa_3 B_z\hat{\mathbf{z}} \\ &+\delta_1\Big\{3\left[(\mathbf{A}^{\uparrow}+\mathbf{A}^{\downarrow})\cdot\hat{\mathbf{r}}_{\rm xy}\right]\hat{\mathbf{r}}_{\rm xy} - \mathbf{A}^{\uparrow} - \mathbf{A}^{\downarrow} \\ &\quad +3\left[(\mathbf{C}^{\uparrow}+\mathbf{C}^{\downarrow})\cdot\hat{\mathbf{r}}_{\bar{\rm x}\rm y}\right]\hat{\mathbf{r}}_{\bar{\rm x}\rm y} - \mathbf{C}^{\uparrow} - \mathbf{C}^{\downarrow}\Big\}\end{aligned} \tag{12}$$

The effective field $\mathbf{F}(\rm D)$ on a D-site is obtained from (12) with the replacements $\mathbf{B}\to\mathbf{D}$, $\mathbf{A}\to\mathbf{C}$ and $\mathbf{C}\to\mathbf{A}$.

IV. LINEARIZATION AROUND A GROUND STATE

Next we consider the small-amplitude magnetic fluctuations around the ground state defined in (3). To accomplish this, the four sublattices are assumed to have

only tranverse deviations from the ground state, denoted as **a, b, c, d**, with amplitudes much smaller than unity. The net unit dipole fields are approximated as

$$\begin{aligned}\mathbf{A} &= \mathbf{A}_0+\mathbf{a}\approx(1,a_y,a_z), &(13a)\\ \mathbf{B} &= \mathbf{B}_0+\mathbf{b}\approx(b_x,1,b_z), &(13b)\\ \mathbf{C} &= \mathbf{C}_0+\mathbf{c}\approx(-1,c_y,c_z), &(13c)\\ \mathbf{D} &= \mathbf{D}_0+\mathbf{d}\approx(d_x,-1,d_z). &(13d)\end{aligned}$$

These are used in the dynamic equations such as (7) and its equivalent on the other sublattices. The equations are linearized, such that any terms quadratic and higher in these deviations are dropped. Longitudinal deviations a_x, b_y, c_x, d_y are zero in the linearized theory. The dynamic equations determine the time derivatives of the eight remaining fluctuation components, that correspond to small-amplitude rotations of the islands' dipoles away from the ground state configuration. Small-amplitude oscillations are those for which angular deviations satisfy $\sin\phi\approx\phi$. On the A-sublattice, one obtains from (7),

$$\begin{aligned}\dot a_y &= \delta_1\left(6a_z+b_z^{\uparrow}+b_z^{\downarrow}+d_z^{\uparrow}+d_z^{\downarrow}\right)\\ &\quad +\kappa_{13}a_z, &(14a)\\ \dot a_z &= \delta_1\left[-6a_y+\tfrac{3}{2}\left(b_x^{\uparrow}+b_x^{\downarrow}-d_x^{\uparrow}-d_x^{\downarrow}\right)\right]\\ &\quad -\kappa_1 a_y. &(14b)\end{aligned}$$

The combination of anisotropy constants appears,

$$\kappa_{13}\equiv\kappa_1+\kappa_3. \tag{15}$$

There are equations of similar structure for the other dynamically fluctuating pairs of transverse components, (b_x,b_z), (c_y,c_z) and (d_x,d_z), but with appropriate symmetry modifications.

A. Traveling wave dynamic modes

The linearized equations can be solved by assuming traveling waves for the small-amplitude fields. For example, on the B-sites, we take

$$b_x(\mathbf{r},t)=b_x e^{i(\mathbf{q}\cdot\mathbf{r}-\omega t)}, \tag{16}$$

where b_x is a complex wave amplitude, $\mathbf{q}=(q_x,q_y)$ is a wave vector and ω is the frequency for that wave vector. The equations contain combinations of the neighbors of a site, which have been labeled by up ($\uparrow$) and down ($\downarrow$) arrows. As these are always along the displacements $\mathbf{r}_{\rm xy}$ and $\mathbf{r}_{\bar x y}$, one gets, for instance,

$$\begin{aligned}b_x^{\uparrow}+b_x^{\downarrow} &= b_x e^{i(\mathbf{q}\cdot\mathbf{r}-\omega t)}\left(e^{i\mathbf{q}\cdot\mathbf{r}_{\rm xy}}+e^{-i\mathbf{q}\cdot\mathbf{r}_{\rm xy}}\right), &(17a)\\ d_x^{\uparrow}+d_x^{\downarrow} &= d_x e^{i(\mathbf{q}\cdot\mathbf{r}-\omega t)}\left(e^{i\mathbf{q}\cdot\mathbf{r}_{\bar x y}}+e^{-i\mathbf{q}\cdot\mathbf{r}_{\bar x y}}\right). &(17b)\end{aligned}$$

The phase factors are denoted as

$$\begin{aligned}u &\equiv e^{i\mathbf{q}\cdot\mathbf{r}_{\rm xy}}+e^{-i\mathbf{q}\cdot\mathbf{r}_{\rm xy}}=2\cos[\tfrac{a}{2}(q_x+q_y)], &(18a)\\ v &\equiv e^{i\mathbf{q}\cdot\mathbf{r}_{\bar x y}}+e^{-i\mathbf{q}\cdot\mathbf{r}_{\bar x y}}=2\cos[\tfrac{a}{2}(q_x-q_y)]. &(18b)\end{aligned}$$

This maps the linearized dynamic equations into an 8×8 eigenvalue problem,

$$\begin{aligned}-i\omega a_y &= \delta_1(6a_z+ub_z+vd_z)+\kappa_{13}a_z, &(19a)\\ -i\omega a_z &= \delta_1(-6a_y+\tfrac{3}{2}ub_x-\tfrac{3}{2}vd_x)-\kappa_1 a_y, &(19b)\\ -i\omega b_x &= \delta_1(-6b_z-ua_z-vc_z)-\kappa_{13}b_z, &(19c)\\ -i\omega b_z &= \delta_1(6b_x-\tfrac{3}{2}ua_y+\tfrac{3}{2}vc_y)+\kappa_1 b_x, &(19d)\\ -i\omega c_y &= \delta_1(-6c_z-ud_z-vb_z)+\kappa_{13}c_z, &(19e)\\ -i\omega c_z &= \delta_1(6c_y-\tfrac{3}{2}ud_x+\tfrac{3}{2}vb_x)-\kappa_1 c_y, &(19f)\\ -i\omega d_x &= \delta_1(6d_z+uc_z+va_z)-\kappa_{13}d_z, &(19g)\\ -i\omega d_z &= \delta_1(-6d_x+\tfrac{3}{2}uc_y-\tfrac{3}{2}va_y)+\kappa_1 d_x. &(19h)\end{aligned}$$

Before eliciting a solution for the general eigenmodes, a physical analysis of the situation points towards the symmetry of the lowest frequency fluctuations.

B. Lowest energy fluctuations

We consider small angular fluctuations of the dipoles within the xy-plane, away from the ground state configuration. A long wavelength mode is assumed, where all the sites on a given lattice rotate nearly in-phase with each other. Consider the dipolar energy contributions around a single vertex of the lattice, see Fig. 2. Small in-plane angular deviations away from the ground state configuration are assumed, one for each sublattice: $\phi_{\rm A},\phi_{\rm B},\phi_{\rm C},\phi_{\rm D}$. Ignoring any small out-of-plane deviations, the unit dipole components for the sites on the different sublattices in one vertex as in Fig. 2 are

$$\begin{aligned}\mathbf{A} &= (\cos\phi_{\rm A},\sin\phi_{\rm A},0), &(20a)\\ \mathbf{B} &= (-\sin\phi_{\rm B},\cos\phi_{\rm B},0), &(20b)\\ \mathbf{C} &= (-\cos\phi_{\rm C},-\sin\phi_{\rm C},0), &(20c)\\ \mathbf{D} &= (\sin\phi_{\rm D},-\cos\phi_{\rm D},0). &(20d)\end{aligned}$$

The AB in-plane dipolar energy in (1) for one vertex is found to be

$$\begin{aligned}\mathcal{H}_{\rm AB}^{\rm dip} &= -\frac{\mathcal{D}}{2}\left\{3\cos(\phi_{\rm A}+\phi_{\rm B})+\sin(\phi_{\rm A}-\phi_{\rm B})\right\}\\ &\approx -\frac{\mathcal{D}}{2}\left\{3+(\phi_{\rm A}-\phi_{\rm B})-\tfrac{3}{2}(\phi_{\rm A}+\phi_{\rm B})^2\right\}. &(21)\end{aligned}$$

In the sine term, increasing $\phi_{\rm A}$ moves the A-dipole towards the direction of the vector $\mathbf{r}_{\rm AB}$, which lowers the energy, while increasing $\phi_{\rm B}$ moves the B-dipole away from the direction of $\mathbf{r}_{\rm AB}$, raising the energy. The in-plane dipolar energy in the BC interaction follows the same rules (positive $\phi_{\rm B}$ moves the B-dipole to be more aligned with $\mathbf{r}_{\rm BC}$, lowering the energy),

$$\begin{aligned}\mathcal{H}_{\rm BC}^{\rm dip} &= -\frac{\mathcal{D}}{2}\left\{3\cos(\phi_{\rm B}+\phi_{\rm C})+\sin(\phi_{\rm B}-\phi_{\rm C})\right\}\\ &\approx -\frac{\mathcal{D}}{2}\left\{3+(\phi_{\rm B}-\phi_{\rm C})-\tfrac{3}{2}(\phi_{\rm B}+\phi_{\rm C})^2\right\}. &(22)\end{aligned}$$

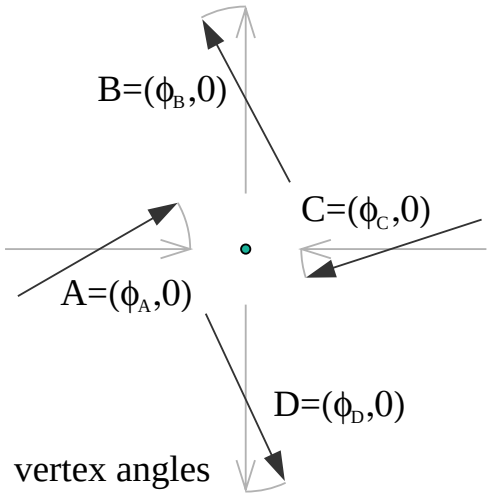

FIG. 2: In-plane deviations away from a ground state (faint gray arrows) in a vertex, drawn with all the angles $\phi_{\rm A}, \phi_{\rm B}, \phi_{\rm C}, \phi_{\rm D}$ positive. This raises the nearest neighbor dipolar energies, Eq. (25).

The CD in-plane dipolar energy in the vertex is lowered for positive $\phi_{\rm C}$,

$$\begin{aligned}\mathcal{H}^{\rm dip}_{\rm CD} &= -\frac{\mathcal{D}}{2}\big\{3\cos(\phi_{\rm C}+\phi_{\rm D})+\sin(\phi_{\rm C}-\phi_{\rm D})\big\}\\ &\approx -\frac{\mathcal{D}}{2}\big\{3+(\phi_{\rm C}-\phi_{\rm D})-\tfrac{3}{2}(\phi_{\rm C}+\phi_{\rm D})^2\big\}. \quad (23)\end{aligned}$$

Finally, the in-plane dipolar energy in the DA interaction is lowered for positive $\phi_{\rm D}$,

$$\begin{aligned}\mathcal{H}^{\rm dip}_{\rm DA} &= -\frac{\mathcal{D}}{2}\big\{3\cos(\phi_{\rm D}+\phi_{\rm A})+\sin(\phi_{\rm D}-\phi_{\rm A})\big\}\\ &\approx -\frac{\mathcal{D}}{2}\big\{3+(\phi_{\rm D}-\phi_{\rm A})-\tfrac{3}{2}(\phi_{\rm D}+\phi_{\rm A})^2\big\}. \quad (24)\end{aligned}$$

Summing these nearest neighbor dipolar energies gives an expression with quadratic terms,

$$\begin{aligned}\mathcal{H}^{\rm dip}_{\rm vertex} \approx \frac{\mathcal{D}}{2}\ \big\{\ &-12+\tfrac{3}{2}\big[(\phi_{\rm A}+\phi_{\rm B})^2+(\phi_{\rm B}+\phi_{\rm C})^2\\ &+(\phi_{\rm C}+\phi_{\rm D})^2+(\phi_{\rm D}+\phi_{\rm A})^2\big]\big\} \quad (25)\end{aligned}$$

Then, if the dipoles rotate in such a way to minimize $\mathcal{H}^{\rm dip}_{\rm vertex}$, the motion must be constrained according to the phase relationships,

$$\phi_{\rm A}=-\phi_{\rm B},\ \phi_{\rm B}=-\phi_{\rm C},\ \phi_{\rm C}=-\phi_{\rm D},\ \phi_{\rm D}=-\phi_{\rm A}. \quad (26)$$

This means that in a low-energy (or low-frequency) mode, neighboring dipoles will tend to move *out-of-phase* with each other. These equations also then imply an *in-phase* relationship across the two diagonals of the vertex:

$$\phi_{\rm A}=\phi_{\rm C}, \quad \phi_{\rm B}=\phi_{\rm D}. \quad (27)$$

Taken together, these conditions would be met, for instance, when in-plane deviations $\phi_{\rm A}$ and $\phi_{\rm C}$ are both positive, while $\phi_{\rm B}$ and $\phi_{\rm D}$ are both negative (or *vice-versa*).

If the in-plane dipolar interactions were the only interactions in the system, such fluctuations would correspond to an acoustic mode in the system, whose frequency goes to zero for zero wave vector. Of course, this system also has anisotropy terms and dipolar interactions of the out-of-plane components, which will give this mode of fluctuation a nonzero frequency. This type of mode should have a minimum frequency for zero wave vector but it will not be at zero frequency. It is expected to become an acoustic mode in the limit of zero easy-axis anisotropy (but that would no longer be a model for spin ice). A mode that has this property will be referred to as an *acoustic-like* mode.

Refering to Fig. 2, the angle constraints (27) for the lowest frequency modes imply that the Cartesian components in (19) have *antisymmetry* across the center of the vertex,

$$a_y=-c_y, \quad b_x=-d_x. \quad (28)$$

We call this mode type *antisymmetric* or type A, referring to the *in-plane* dipolar deviations across the center of a vertex. On the other hand, the other angular constraints (26) imply for the Cartesian components of nearest neighbor dipoles,

$$a_y=b_x, \quad c_y=d_x. \quad (29)$$

To get these antisymmetric modes, we combine the constraints on the in-plane deviations with a phase relation (39) below for the out-of-plane components that results from consideration of the precessional dipolar motions.

The linearized energy in a vertex also includes dipolar energy in the out-of-plane components, and the anisotropy energy that was initially not taken into account in (25). When those terms are included, the total energy change away from the ground state is found to be

$$\begin{aligned}\mathcal{H}_{\rm vertex} \approx\ &\frac{\mathcal{D}}{2}\big\{-12+\tfrac{3}{2}\big[(\phi_{\rm A}+\phi_{\rm B})^2+(\phi_{\rm B}+\phi_{\rm C})^2\\ &+\ (\phi_{\rm C}+\phi_{\rm D})^2+(\phi_{\rm D}+\phi_{\rm A})^2\big]\\ &+\ (a_z+c_z)(b_z+d_z)\big\}\\ &+\ K_1(a_y^2+b_y^2+c_y^2+d_y^2)\\ &+\ (K_1+K_3)(a_z^2+b_z^2+c_z^2+d_z^2). \quad (30)\end{aligned}$$

The anisotropy terms produce a nonzero frequency even at small wave vector. More interesting are the dipolar terms involving the z-components, $(a_z+c_z)(b_z+d_z)$. Those can be zeroed out, but not necessarily minimized, by assuming opposite phases across the vertex:

$$a_z=-c_z, \quad b_z=-d_z. \quad (31)$$

However, another possibility that could give even a negative energy contribution is if the z-components are in-phase across the vertex,

$$a_z=c_z, \quad b_z=d_z, \quad (32)$$

together with an opposite phase relation such as $a_z = -b_z$. The selection of one of these possibilities is decided next by analyzing the precessional spin dynamics.

C. Low energy precessional motion

The choice of phase relationship for the z-components in a low energy mode was not determined in the energy analysis. Expressions (31) and (32) both give low energy, without accounting for the dynamics. But some insight can be found by a comparison to the phase relationships that are present for spin wave modes in one-dimensional (1D) antiferromagnets, which require a two-sublattice model. Looking across a vertex, the A and C sites in the spin ice ground state alternate in direction just as in a 1D antiferromagnet, which has both acoustic and optical modes. The torque equation (4) shows that in a small time interval δt, the change in the A-site dipole results from precession in the left hand sense around its effective field $\mathbf{F}(\mathrm{A})$,

$$\delta\mathbf{A} \approx \mathbf{A} \times \mathbf{F}(\mathrm{A})\, \delta t. \tag{33}$$

From (10), the effective field for the A-site is dominated by its x-component,

$$\mathbf{F}(\mathrm{A}) \approx (6\delta_1 + \kappa_1, 0, 0). \tag{34}$$

With $\mathbf{A} \approx (1, a_y, a_z)$, this gives

$$\delta\mathbf{A} \approx (6\delta_1 + \kappa_1)\delta t\, (0, a_z, -a_y). \tag{35}$$

By similar reasoning, a neighboring C-site precesses in the left hand sense around its effective field, which is predominantly in the $-x$ direction,

$$\mathbf{F}(\mathrm{C}) \approx (-6\delta_1 - \kappa_1, 0, 0). \tag{36}$$

With $\mathbf{C} \approx (-1, c_y, c_z)$, one has

$$\delta\mathbf{C} \approx (6\delta_1 + \kappa_1)\delta t\, (0, -c_z, c_y). \tag{37}$$

From (28) for low energy modes, using the relation $a_y = -c_y$ in the expression for $\delta\mathbf{C}$ gives

$$\delta\mathbf{C} \approx (6\delta_1 + \kappa_1)\delta t\, (0, -c_z, -a_y). \tag{38}$$

This shows that both the changes $\delta\mathbf{A}$ and $\delta\mathbf{C}$ across the center of a vertex could have identical z-components for a low energy mode. Further, their y-components also are consistent with $\mathbf{A}$ and $\mathbf{C}$ having equal z-components. Thus we should expect that any *antisymmetric* mode should have an in-phase relation for the out-of-plane components:

$$a_z = c_z, \quad b_z = d_z. \tag{39}$$

This should apply in conjunction with relations (28) and (29) for the in-plane components. A sketch of the expected small deviations in one vertex for a lowest energy antisymmetric mode is given in Fig. 3. Both the A and C sublattices would rotate synchronized in-plane, in the same direction ($\phi_{\mathrm{A}} = \phi_{\mathrm{C}}$), and they would also both tilt out of the xy-plane with in-phase z-components. The B and D sublattices would move together in the opposite sense compared to A and C, for both the in-plane and out-of-plane components. These motions can be seen to minimize the linearized nearest neighbor dipolar energy changes within the vertex, see Eq. (30). These are the type of phase relationships present between the two sublattices in the acoustic modes of a 1D antiferromagnet.

D. Finding the antisymmetric modes

For the antisymmetric modes, the fields on two sublattices can be eliminated by imposing the expected antisymmetric constraints from (28) and (39), summarized together here:

$$a_y = -c_y, \qquad a_z = c_z, \tag{40a}$$
$$b_x = -d_x, \qquad b_z = d_z. \tag{40b}$$

This reduces the original 8×8 system (19) to four 2×2 systems, one for each sublattice, with the same possible eigenfrequencies:

$$\omega_{A^\pm}^2 = (\alpha_1\alpha_2 + \tfrac{3}{2}\gamma_+^2) \pm \gamma_+(\alpha_1 + \tfrac{3}{2}\alpha_2). \tag{41}$$

The new frequency constants are

$$\alpha_1 \equiv \kappa_1 + 6\delta_1, \quad \alpha_2 \equiv \kappa_{13} + 6\delta_1, \tag{42a}$$
$$\gamma_+ \equiv \delta_1(u+v) = 4\delta_1 \cos(\tfrac{1}{2}q_x a)\cos(\tfrac{1}{2}q_y a). \tag{42b}$$

A little consideration shows that for small wave vector, ω_{A^-} is the lower of the two frequencies, and it goes to zero as $q \to 0$ when no uniaxial anisotropy is present ($\kappa_1 = \kappa_3 = 0$). The frequency ω_{A^+} tends to a large nonzero value at zero wave vector. Eq. (41) gives solutions for four of the eight possible modes of the original 8×8 system in Eq. (19), because a chosen wave vector $\mathbf{q}$ has frequencies $\pm\omega_{\mathrm{A}^-}$ and $\pm\omega_{\mathrm{A}^+}$, due to oppositely directed traveling waves being possible. The modes' frequencies can be written as products:

$$\omega_{A^-}^2 = \left(\alpha_1 - \tfrac{3}{2}\gamma_+\right)(\alpha_2 - \gamma_+), \tag{43a}$$
$$\omega_{A^+}^2 = \left(\alpha_1 + \tfrac{3}{2}\gamma_+\right)(\alpha_2 + \gamma_+). \tag{43b}$$

The factor $\left(\alpha_1 - \frac{3}{2}\gamma_+\right)$ tends to zero in the simultaneous limit of zero wave vector and zero anisotropy, making it obvious that ω_{A^-} is an acoustic-like mode.

1. Mode A^- eigenvector and features

For the mode at frequency ω_{A^-} we can also look at the structure of its eigenvector, in terms of the phase relationships between the different dipolar components.

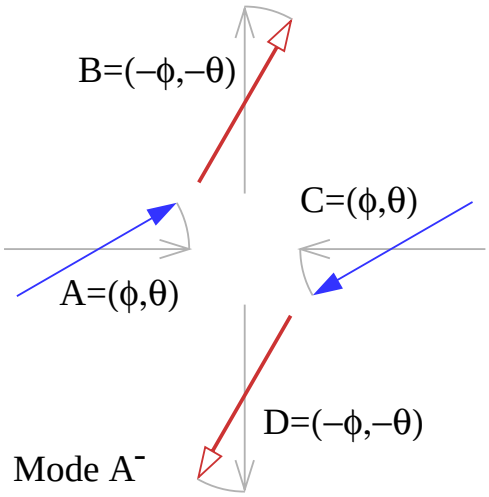

FIG. 3: Phase relationships of the dipolar angles expected in the antisymmetric mode denoted as A^-, with in-plane rotations having $\phi_{\rm A} = -\phi_{\rm B} = \phi_{\rm C} = -\phi_{\rm D}$, and out-of-plane components obeying $a_z = -b_z = c_z = -d_z$. A and C rotate in the same in-plane direction and tilt positively out of plane together; B and D rotate together oppositely to A and C, and tilt out of plane together oppositely to A and C. These motions minimize the nearest neighbor dipolar energy changes, see Eq. (30). This mode becomes acoustic-like in the limit of zero wave vector and zero anisotropy.

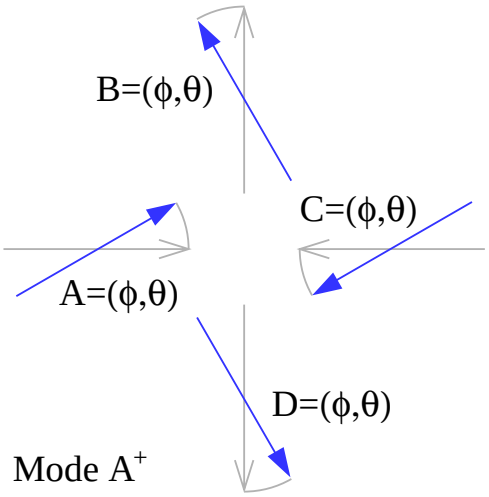

FIG. 4: Phase relationships of the dipolar angles expected in the antisymmetric mode denoted $\rm A^+$, with frequency $\omega_{\rm A^+}$ given in Eq. (43b). The in-plane rotations are equal and in-phase: $\phi_{\rm A} = \phi_{\rm B} = \phi_{\rm C} = \phi_{\rm D}$, and the out-of-plane components are also equal and in-phase: $a_z = b_z = c_z = d_z$. These motions tend to cause large changes in the nearest neighbor dipolar energies, see Eq. (30).

For its in-plane components, when frequency ω_{A^-} is used in Eq. (19), one finds an in-phase relation for in-plane components of neighbors,

$$a_y = b_x, \quad c_y = d_x. \tag{44}$$

and oppposite phase for out-of-plane components,

$$a_z = -b_z, \quad c_z = -d_z. \tag{45}$$

A snapshot of the angular deviations for the $\rm A^-$ mode is given in Fig. 3, and its time-dependent oscillations are animated in the Supplementary Material[24]. All in-plane angular deviations are of the same magnitudes, but with opposite phases between neighboring dipoles. All out-of-plane deviations are also of equal magnitudes, but with opposite phases between neighboring dipoles. The deviations on each sublattice can be summarized in an eigenvector with Cartesian component pairs on each sublattice,

$$\psi = (a_y, a_z,\ b_x, b_z,\ c_y, c_z,\ d_x, d_z). \tag{46}$$

For this lowest (acoustic-like) antisymmetric mode, the eigenvector is

$$\psi_{A^-} = (a_y, a_z,\ a_y, -a_z,\ -a_y, a_z,\ -a_y, -a_z), \tag{47}$$

determined by just two components. Using $b_z = -a_z$ in Eq. (19), the relation between those components is

$$a_z = \frac{-{\rm i}\omega_{A^-}}{(\alpha_2 - \gamma_+)} a_y = -{\rm i}\left(\frac{\alpha_1 - \frac{3}{2}\gamma_+}{\alpha_2 - \gamma_+}\right)^{\frac{1}{2}} a_y. \tag{48}$$

In the acoustic-like limit of zero wave vector and zero anisotropy, a_z tends towards zero, and the motion is predominantly in-plane.

2. *Mode A^+ eigenvector and features*

For the mode at the higher frequency, ω_{A^+}, we expect different relative motions of the sublattices. For in-plane components, when frequency ω_{A^+} is used in Eq. (19), we arrive at opposite phases for neighboring dipoles,

$$a_y = -b_x, \quad c_y = -d_x. \tag{49}$$

When combined with the assumptions in Eq. (40), this shows that all of the in-plane angles move together in-phase ($\phi_{\rm A} = \phi_{\rm B} = \phi_{\rm C} = \phi_{\rm D}$). One also finds in-phase motions for the out-of-plane components,

$$a_z = b_z, \quad c_z = d_z. \tag{50}$$

Together with (40), this implies that all out-of-plane components move in-phase. As defined in (46), the eigenvector for this mode is

$$\psi_{A^+} = (a_y, a_z,\ -a_y, a_z,\ -a_y, a_z,\ a_y, a_z). \tag{51}$$

A snapshot of the deviation structure is given in Fig. 4, and the motion is animated in the Supplementary Material[24]. These angular deviations of the dipoles tend to raise their nearest neighbor dipolar energy; this is not an acoustic-like mode in the limit of zero anisotropy

and wave vector. As far as the relative magnitudes of in-plane vs. out-of-plane components, one finds

$$a_z = \frac{-\mathrm{i}\omega_{A+}}{(\alpha_2+\gamma_+)}a_y = -\mathrm{i}\left(\frac{\alpha_1+\frac{3}{2}\gamma_+}{\alpha_2+\gamma_+}\right)^{\frac{1}{2}} a_y. \qquad (52)$$

In the limit of zero wave vector and zero anisotropy, the a_z and a_y components have similar amplitudes.

E. Finding the symmetric modes

Contrary to the assumptions made in Eq. (40) for the antisymmetric modes, it is reasonable to assume that there are modes whose in-plane Cartesian components are *symmetric* viewed across the center of a vertex,

$$a_y = c_y, \qquad a_z = -c_z, \qquad (53a)$$
$$b_x = d_x, \qquad b_z = -d_z. \qquad (53b)$$

These are the same phase relationships that hold in the optic modes of a 1D antiferromagnet. It is straightforward to show that they do indeed lead to solutions of the original 8×8 system in Eq. (19).

Using (53) to eliminate two of the sublattices, there results from (19) a set of four 2×2 systems, one for each sublattice, whose eigenfrequencies represent the four remaining modes of the original 8×8 system,

$$\omega^2_{S-} = \left(\alpha_1-\tfrac{3}{2}\gamma_-\right)\left(\alpha_2-\gamma_-\right), \qquad (54a)$$
$$\omega^2_{S+} = \left(\alpha_1+\tfrac{3}{2}\gamma_-\right)\left(\alpha_2+\gamma_-\right). \qquad (54b)$$

This involves another wave vector dependent factor,

$$\gamma_- \equiv \delta_1(u-v) = -4\delta_1 \sin(\tfrac{1}{2}q_x a)\sin(\tfrac{1}{2}q_y a). \qquad (55)$$

This factor becomes identically zero if $q_x = 0$ or $q_y = 0$. Thus, the only symmetric modes that will have some wave vector dependent features will not have wave vector aligned with one of the lattice axes. In the small wave vector limit, we have $\gamma_- \approx -q_x q_y a^2$. These modes have an optic-like character, with a finite frequency at zero wave vector even in the limit of zero anisotropy.

1. *Mode S^- eigenvector and features*

For the mode with frequency ω_{S^-}, substitution of the frequency into the equations of motion gives the relations

$$a_y = b_x, \quad c_y = d_x \quad a_z = -b_z, \quad c_z = -d_z. \qquad (56)$$

These are the same nearest neighbor phase relations as for the mode A^-. Taken together with the symmetric assumption (53), the eigenvector in Cartesian components is of the form

$$\psi_{S^-} = (a_y, a_z,\ a_y, -a_z,\ a_y, -a_z,\ a_y, a_z). \qquad (57)$$

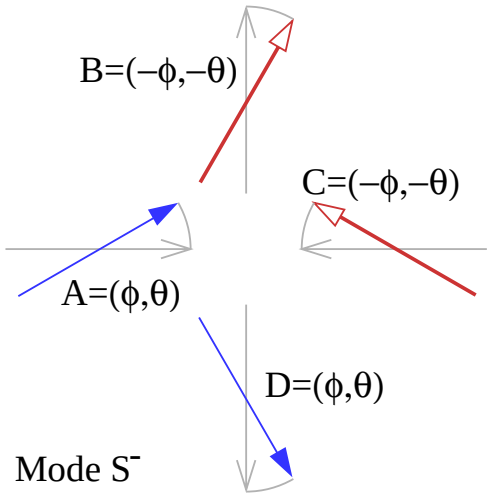

FIG. 5: Phase relationships of the dipolar angles expected in the symmetric mode denoted S^-, with frequency ω_{S^-} given in Eq. (54a). The in-plane angular deviations are towards the same side for dipole pairs across the vertex center. The out-of-plane deviations are in opposite directions across the vertex center. The nearest neighbor relative deviations are partly energy reducing and partly energy enhancing.

By using $a_z = -b_z$ in Eq. (19), one arrives at the phase relation between in-plane and out-of-plane components,

$$a_z = \frac{-\mathrm{i}\omega_{S^-}}{(\alpha_2-\gamma_-)}a_y = -\mathrm{i}\left(\frac{\alpha_1-\frac{3}{2}\gamma_-}{\alpha_2-\gamma_-}\right)^{\frac{1}{2}} a_y. \qquad (58)$$

A snapshot of the deviations in a vertex is shown in Fig. 5, and the motion is animated in the Supplementary Material[24]. Out of the four dipole-pair interactions, two of them reduce their energy while two of them increase their energy, compared to the ground state. The AB and CD couplings move towards lower energy while the BC and DA couplings have moved towards higher energy.

2. *Mode S^+ eigenvector and features*

For the mode with frequency ω_{S^+}, substitution of the frequency into the equations of motion gives the relations,

$$a_y = -b_x, \quad c_y = -d_x \quad a_z = b_z, \quad c_z = d_z. \qquad (59)$$

These are the same nearest neighbor phase relations as for the mode A^+. Together with the symmetric assumption (53), the eigenvector in Cartesian components is of the form

$$\psi_{S^+} = (a_y, a_z,\ -a_y, a_z,\ a_y, -a_z,\ -a_y, -a_z). \qquad (60)$$

By using $a_z = b_z$ in Eq. (19), one arrives at the phase relation between in-plane and out-of-plane components,

$$a_z = \frac{-\mathrm{i}\omega_{S^+}}{(\alpha_2+\gamma_-)}a_y = -\mathrm{i}\left(\frac{\alpha_1+\frac{3}{2}\gamma_-}{\alpha_2+\gamma_-}\right)^{\frac{1}{2}} a_y. \qquad (61)$$

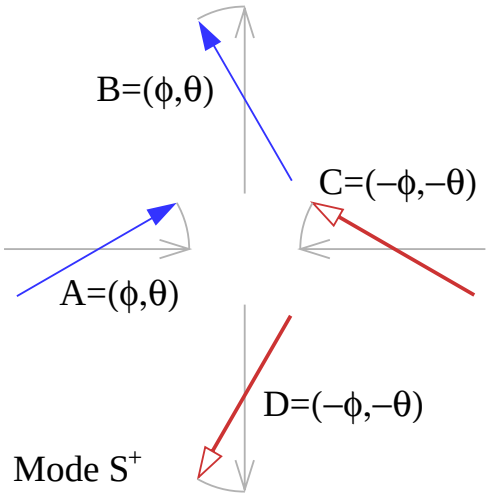

FIG. 6: Phase relationships of the dipolar angles expected in the symmetric mode denoted S^+, with frequency ω_{S^+} given in Eq. (54b). The in-plane angular deviations are towards the same side for dipole pairs across the vertex center. The out-of-plane deviations are in opposite directions across the vertex center. The nearest neighbor relative deviations are partly energy reducing and partly energy enhancing.

A snapshot of the deviations in a vertex is shown in Fig. 6, and the motion is animated in the Supplementary Material[24]. In a certain sense it is very similar to the mode S^-. Out of the four dipole-pair interactions, again two reduce their energy while two increase their energy. The AB and CD couplings move towards higher energy while the BC and DA couplings have moved towards lower energy, opposite to what takes place in mode S^-.

Indeed, there isn't a significant difference between modes S^+ and S^-, due to the behavior of the factor γ_-, which reverses sign with a change in sign of either q_x or q_y, see Eq. (55). One can see $\omega_{S^-} \to \omega_{S^+}$ under a change such as $q_x \to -q_x$ or $q_y \to -q_y$. Thus, the two modes map into each other with an appropriate change of wave vector.

V. POSSIBLE EXCITATION SPECTRA

Here we calculate some spectra for the excitations in a couple of situations. The anisotropy constants κ_1, κ_3, and κ_{13} as well as the dipolar coupling δ_1 depend on the specific geometry of the islands. In a typical artificial spin ice, it is likely that the anisotropy constants dominate over the dipolar coupling. Even so, it is instructive to consider some different choices of these parameters to observe how they affect the mode frequencies.

For convenience here, frequencies will be measured in units of δ_1. We assume elliptical islands like those studied by Wang *et al.* [3] with length $L_x = 220$ nm, width $L_y = 80$ nm and thickness $L_z = 25$ nm. If the material is

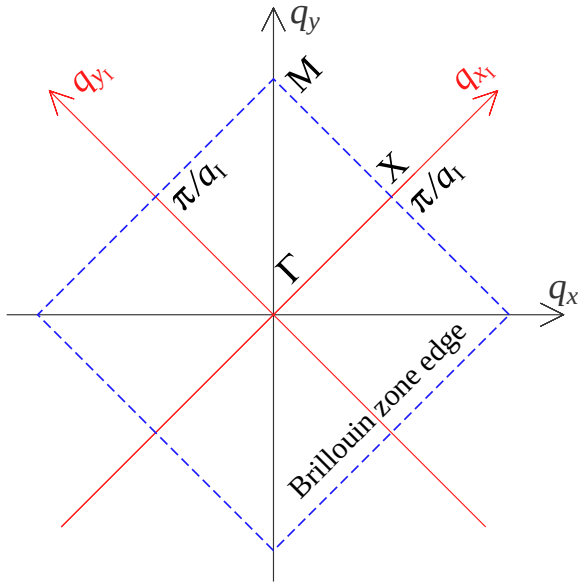

FIG. 7: The first Brillouin zone for the square lattice of magnetic islands, whose near neighbor spacing at 45° from the x-axis is $a_I = a/\sqrt{2}$.

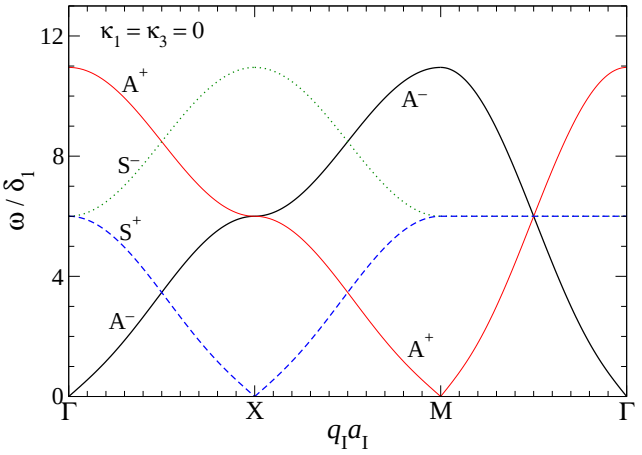

FIG. 8: The excitation spectrum in the limit of zero anisotropy ($\kappa_1 = \kappa_3 = 0$) for wave vectors in the island coordinates from $\Gamma \to X \to M$ in the Brillouin zone, Fig. 7. Modes S^- and S^+ are degenerate along $M \to \Gamma$. Mode A^- is acoustic-like at $\mathbf{q} \to \Gamma$, while its sister-mode A^+ acquires zero frequency at the M-point.

Permalloy with saturation magnetization $M_s = 860$ kA m^{-1}, the dipole moment per island is $\mu = 2.97 \times 10^{-16}$ A m^2, see Wysin *et al.* [12]. We take a lattice constant $a = 320$ nm, then the dipolar coupling constant from Eq. (2) is $\mathcal{D} \approx 7.6 \times 10^{-19}$ J. Using the electron gyromagnetic ratio $\gamma_e = 1.76 \times 10^{11}$ T^{-1} s^{-1}, Eq. (9) gives the value of the dipolar angular frequency constant, $\delta_1 \approx 4.5 \times 10^8$ s^{-1}, corresponding to a frequency unit $\delta_1/2\pi \approx 72$ MHz.

The original xy coordinate system was selected for finding the eigenmodes because the islands are oriented

along those axes, however, the unit vectors of the island lattice are

$$\hat{x}_{\rm I} \equiv \tfrac{1}{\sqrt{2}}(\hat{x}+\hat{y}), \qquad \hat{y}_{\rm I} \equiv \tfrac{1}{\sqrt{2}}(-\hat{x}+\hat{y}). \tag{62}$$

These are the directions of $\mathbf{r}_{xy}$ (45°) and $\mathbf{r}_{\bar{x}y}$ (135°) in Fig. 1. Then the dispersion relations for the modes should be calculated with wave vectors $\mathbf{q} = (q_{x_{\rm I}}, q_{y_{\rm I}})$ expressed in this rotated coordinate system, within the first Brillouin zone, as sketched in Fig. 7. Then the rotated components are

$$q_{x_{\rm I}} = \tfrac{1}{\sqrt{2}}(q_x+q_y), \qquad q_{y_{\rm I}} = \tfrac{1}{\sqrt{2}}(-q_x+q_y). \tag{63}$$

The phase factors used earlier in (18) are now simply $u = 2\cos(q_{x_{\rm I}}a_{\rm I})$ and $v = 2\cos(q_{y_{\rm I}}a_{\rm I})$, where $a_{\rm I} = a/\sqrt{2}$ is the near neighbor distance on the island lattice. This implies simplified phase factors in the dispersion relations,

$$\gamma_+ = \delta_1(u+v) = 2\delta_1[\cos q_{x_{\rm I}}a_{\rm I} + \cos q_{y_{\rm I}}a_{\rm I}], \tag{64a}$$
$$\gamma_- = \delta_1(u-v) = 2\delta_1[\cos q_{x_{\rm I}}a_{\rm I} - \cos q_{y_{\rm I}}a_{\rm I}]. \tag{64b}$$

These were used in dispersion relations (43) for $A^{\pm}$ modes and (54) for $S^{\pm}$ modes to obtain the mode spectra for several situations.

A. Zero anisotropy limit

Initially, consider the extreme limit where the anisotropy constants are zero: $\kappa_1 = \kappa_3 = 0$, and only nearest neighbor dipolar coupling is present. The resulting spectrum for the modes is shown in Fig. 8. The antisymmetric mode A^- is the acoustic-like mode, going to zero frequency linearly at zero wave vector. The other antisymmetric mode, A^+, has its maximum frequency $\omega_{A^+} = \sqrt{120}\delta_1$ at $\mathbf{q} = 0$ (Γ), but linearly acquires zero frequency at the M-point, where mode A^- has its maximum frequency. The symmetric modes are degenerate from M to Γ, or what corresponds to either having $q_x = 0$ or $q_y = 0$ in the original vertex coordinate system. Along Γ to X, however, the S^+ and S^- frequencies move in opposite directions, with ω_{S^-} being higher. If one were to consider wave vectors from Γ to Y (not shown), a similar structure would appear but with ω_{S^+} being higher. As mentioned earlier, modes S^- and S^+ map into each other, because the function γ^- reverses sign if q_x or q_y is reversed in sign, which then takes ω_{S^+} into ω_{S^-} and *vice-versa*. Overall, one sees that there are several wave vector regions with a high density of low-energy modes present, of different symmetries.

B. Weak island anisotropy

Next, we suppose that the islands have weak shape anisotropies with energy constants $K_1 = 0.1\mathcal{D}$ and $K_3 = 0.5\mathcal{D}$, but still with the same values of dipolar moment $\mu = 2.97\times10^{-16}$ A m^2 and dipolar angular frequency $\delta_1 = 4.5\times10^8$ s^{-1}.

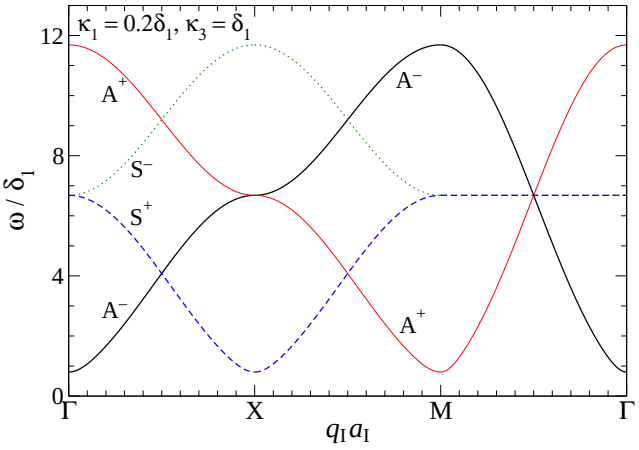

FIG. 9: The excitation spectrum for weak anisotropy, with $\kappa_1 = 0.2\delta_1$ and $\kappa_3 = \delta_1$ for wave vectors in the first Brillouin zone of the island lattice. Note the small gap that opens up in the spectrum, of size $\omega_{\rm gap} = \sqrt{\kappa_1(\kappa_{13}+2\delta_1)} = 0.8\delta_1$.

Then the scaled anisotropy factors from Eq. (9) are $\kappa_1 = 0.2\delta_1$ and $\kappa_3 = \delta_1$, which also gives $\kappa_{13} = 1.2\delta_1$. The mode spectrum that results is shown in Fig. 9. In the limit of small wave vector, a gap opens at $\mathbf{q} = 0$ in the A^- spectrum, given by

$$\omega_{\rm gap} = \omega_{A^-}(0) = \sqrt{\kappa_1(\kappa_{13}+2\delta_1)}. \tag{65}$$

For the chosen parameters, the gap is $\omega_{\rm gap} = 0.8\delta_1$. The same gap opens up for mode S^+ at X, mode S^- at Y, and for mode A^- at the M points. Now the acoustic-like mode is only weakly linear at long wavelength; the dispersion relations very near the frequency minima depend quadratically on the deviations of $\mathbf{q}$.

C. Realistic anisotropy in a spin ice

Finally it is important to show a prediction from this model for realistic parameters of typical islands in artificial square spin ice, such as that studied by Wang *et al.* [3]. Assuming elliptical islands with length $L_x = 220$ nm, width $L_y = 80$ nm and thickness $L_z = 25$ nm, energy minimization simulations indicate that their dipoles behave in a way described with easy-axis anisotropy parameter $K_1 \approx 2.9\times10^{-17}$ J and hard-axis anisotropy parameter $K_3 = 6.4\times10^{-17}$ J. For lattice parameter $a = 320$ nm, we found above the dipolar energy constant $\mathcal{D} \approx 7.6\times10^{-19}$ J. Then Eq. (9) implies the anisotropy frequency constants are

$$\kappa_1 \approx 76\delta_1, \quad \kappa_3 \approx 168\delta_1, \quad \kappa_{13} \approx 244\delta_1. \tag{66}$$

As expected, the anisotropy is very strong compared to the dipolar interactions. This leads to a substantial gap

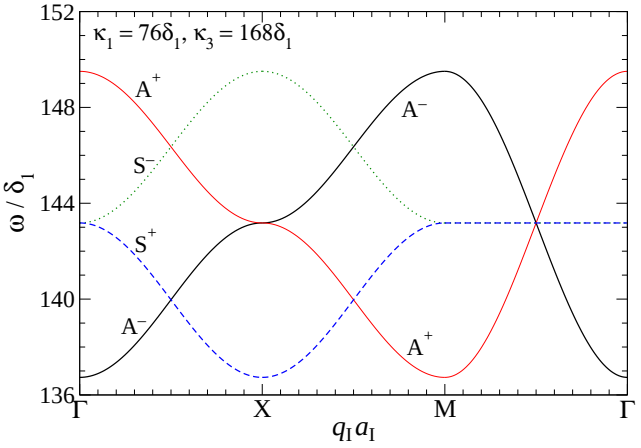

FIG. 10: The excitation spectrum for realistic anisotropy in a spin ice, with $\kappa_1 = 76\delta_1$ and $\kappa_3 = 168\delta_1$, for wave vectors in the first Brillouin zone of the island lattice. The spectrum is strongly elevated by a gap of size $\omega_{\rm gap} = \sqrt{\kappa_1(\kappa_{13} + 2\delta_1)} = 136.7\delta_1$, but otherwise similar to that at weak anisotropy.

in the spectrum,

$$\omega_{\rm gap} = \sqrt{\kappa_1(\kappa_{13} + 2\delta_1)} \approx 136.7\delta_1. \qquad (67)$$

The resulting spectrum is shown in Fig. 10. One can see that the **q**-dependence of the mode frequencies resembles that for weak anisotropy, except that the entire spectrum is elevated an amount equal to the gap frequency. The variations in the mode frequencies with **q** are a rather small fraction of the total frequency.

VI. DISCUSSION AND CONCLUSIONS

The eigenfrequencies and eigenvectors for four different types of modes have been found analytically by diagonalization of the dynamic matrix for the model. In the modes denoted as *antisymmetric*, the in-plane dipole components across the center of one vertex move oppositely. For mode A^-, both the in-plane and out-of-plane components of two nearest neighbor dipoles such as AB or AD also move oppositely relative to each other, see Fig. 3. To the contrary, for mode A^+, both the in-plane and out-of-plane components of two nearest neighbor dipoles move or rotate together in the same sense, see Fig. 4. For $\mathbf{q} \to 0$, the frequency of mode A^- goes to a minimum; if no anisotropy is present, that minimum frequency goes to zero linearly with **q**, and mode A^- is acoustic-like. An energy analysis for long wave vectors (Sec. IV B) aided greatly in pointing towards the properties and phase relationships of the in-plane components of the mode that becomes acoustic-like. An associated analysis of the precessional motion of a dipole (Sec. IV C) also was essential for understanding the phase relationships needed for the out-of-plane dipole components for the lowest energy modes. These symmetry considerations reduced the problem to separated 2×2 matrices for each of the four mode branches.

In the other modes denoted as *symmetric*, the in-plane dipole components across the center of one vertex move in the same direction. Depending on the choice of wave vector and especially its direction, one of the modes S^- or S^+ may also go to low frequency in the limit of zero anisotropy. That is because their frequencies ω_{S-} and ω_{S+} get interchanged when the wave vector dependent factor γ_- reverses sign, see Eq. (54). This sign reversal would occur, for instance, by changing $q_x \to -q_x$ or by $q_y \to -q_y$ (but not both together). Indeed, a similar effect is present for the frequencies ω_{A-} and ω_{A+} of modes A^- and A^+, see Eq. (43), if the sign of the wave vector dependent factor γ_+ is reversed.

For nonzero anisotropy factors K_1 and K_3, a gap opens at the bottom of the spectrum, given by Eq. (65); mode A^- acquires a finite frequency as $\mathbf{q} \to 0$. The gap becomes significant for realistic anisotropy constants that might be expected for typical elongated spin ice islands. Still, there will be a **q**-dependent modulation of the mode frequencies whose amplitude depends on the nearest neighbor dipolar coupling, characterized by the dipolar frequency δ_1.

The spectra found here ignore magnetization dynamics within the islands, thus the frequencies are higher than those in the semi-analytic calculations by Iacocca *et al.* [17] and others [18, 20]. We are not considering that any islands' dipoles rotate so far as to execute a reversal. The nearest-neighbor approximation ignores the long range of dipolar interactions, which facilitated the analytic solutions while slightly reducing the calculated frequencies. As a result, we cannot expect the dependence of frequency results on the dipolar frequency δ_1 (due to nearest neighbors only) to be completely correct. The modes found should give some idea of the likely oscillatory motions, but the numerical details are approximate. On the other hand, the dependencies of the mode frequencies on the anisotropy constants such as κ_1 and κ_3, being local energy parameters, should be more reliable. Accounting for interactions beyond nearest neighbors will be the topic of a future study.

Ultimately, knowledge of the spin wave modes in artificial spin ice may be useful for identifying differences between a ground and other states. The presence of monopoles in excited states would modify the spectrum[18] as the spin waves would scatter from monopoles. That effect is likely to broaden each mode frequency. Calculations such as those presented here may be useful also for indicating the frequencies and polarization properties of applied magnetic fields intended to manipulate artificial spin ice states.

[1] S.H. Skjærvø, C.H. Marrows, R.L. Stamps and L.J. Heyderman, Nat. Rev. Phys. **2**, 13–28 (2020).

[2] C. Nisoli, R. Moessner, and P. Schiffer, Rev. Mod. Phys. **85**, 1473 (2013).

[3] R.F. Wang, C. Nisoli, R.S. Freitas, J. Li, W. McConville, B.J. Cooley, M.S. Lund, N. Samarth, C. Leighton, V.H. Crespi and P. Schiffer, Nature **439**, 303 (2006).

[4] J.P. Morgan, A. Stein, S. Langridge, and C. Marrows, Nature Phys. **7**, 75 (2011).

[5] G. Möller and R. Moessner Phys. Rev. Lett. **96**, 237202 (2006).

[6] Alan Farhan, Michael Saccone, Charlotte F. Petersen, Scott Dhuey, Rajesh V. Chopdekar, Yen-Lin Huang, Noah Kent, Zuhuang Chen, Mikko J. Alava, Thomas Lippert, Andreas Scholl and Sebastiaan van Dijken, Sci. Adv. **5**, eaav6380 (2019).

[7] L.A.S. Mól, R.L. Silva, R.C. Silva, A.R. Pereira, W.A. Moura-Melo, and B.V. Costa, J. Appl. Phys. **106**, 063913 (2009).

[8] L.A.S. Mól, W.A. Moura-Melo, and A.R. Pereira, Phys. Rev. B **82**, 054434 (2010).

[9] G. Möller and R. Moessner, Phys. Rev. B **80**, 140409(R) (2009).

[10] R.C. Silva, F.S. Nascimento, L.A. S. Mól, W.A. Moura-Melo, and A.R. Pereira, New J. Phys. **14**, 015008 (2012).

[11] G.M. Wysin, W.A. Moura-Melo, L.A.S. Mól and A.R. Periera, J. Phys.: Condens. Matter **24** 296001 (2012).

[12] G.M. Wysin, W.A. Moura-Melo, L.A.S. Mól and A.R. Pereira, New J. Phys. **15**, 045029 (2013).

[13] J. Li, X. Ke, S. Zhang, D. Garand, C. Nisoli, P. Lammert, V.H. Crespi, and P. Schiffer, Phys. Rev. B **81**, 092406 (2010).

[14] C. Nisoli, J. Li, X. Ke, D. Garand, P. Schiffer, and V.H. Crespi, Phys. Rev. Lett. **105**, 047205 (2010).

[15] J M Porro, A Bedoya-Pinto, A Berger and P Vavassori, New J. Phys. **15**, 055012 (2013).

[16] A. Farhan, P.M. Derlet, A. Kleibert, A. Balan, R.V. Chopdekar, M. Wyss, J. Perron, A. Scholl, F. Nolting, and L.J. Heyderman, Phys. Rev. Let. **111**, 057204 (2013).

[17] Ezio Iacocca, Sebastian Gliga, Robert L. Stamps, and Olle Heinonen, Phys. Rev. B **93**, 134420 (2016).

[18] Sebastian Gliga, Attila Kákay, Riccardo Hertel, and Olle G. Heinonen, Phys. Rev. Lett. **110**, 117205 (2013).

[19] M. B. Jungfleisch, W. Zhang, E. Iacocca, J. Sklenar, J. Ding, W. Jiang, S. Zhang, J. E. Pearson, V. Novosad, J. B. Ketterson, O. Heinonen, and A. Hoffmann, Phys. Rev. B **93**, 100401(R) (2016).

[20] D. M. Arroo, J. C. Gartside, and W. R. Branford, Phys. Rev. B **100**, 214425 (2019).

[21] G.M. Wysin, A.R. Pereira, W.A. Moura-Melo and C.I.L. de Araujo, J. Phys.: Condens. Matter **27** (7), 076004 (2015).

[22] N. Rougemaille, F. Montaigne, B. Canals, A. Duluard, D. Lacour, M. Hehn, R. Belkhou, O. Fruchart, S. El Moussaoui, A. Bendounan, and F. Maccherozzi, Phys. Rev. Lett. **106**, 057209 (2011).

[23] Y. Shevchenko, A Makarov and K. Nefedev, Physics Letters A, **381(5)**, 428-434 (2017).

[24] See Supplematary Material at [URL to be defined], where the oscillations of the four sublattices surrounding one vertex are animated for small wave vector, showing their symmetry properties.